

DNA nanodevices map enzymatic activity in organelles

Krishna Dan^{1,2}, Aneesh T. Veetil^{1,2}, Kasturi Chakraborty^{1,2} and Yamuna Krishnan^{1,2*}

Cellular reporters of enzyme activity are based on either fluorescent proteins or small molecules. Such reporters provide information corresponding to wherever inside cells the enzyme is maximally active and preclude minor populations present in subcellular compartments. Here we describe a chemical imaging strategy to selectively interrogate minor, subcellular pools of enzymatic activity. This new technology confines the detection chemistry to a designated organelle, enabling imaging of enzymatic cleavage exclusively within the organelle. We have thus quantitatively mapped disulfide reduction exclusively in endosomes in *Caenorhabditis elegans* and identified that exchange is mediated by minor populations of the enzymes PDI-3 and TRX-1 resident in endosomes. Impeding intra-endosomal disulfide reduction by knocking down TRX-1 protects nematodes from infection by *Corynebacterium diphtheriae*, revealing the importance of this minor pool of endosomal TRX-1. TRX-1 also mediates endosomal disulfide reduction in human cells. A range of enzymatic cleavage reactions in organelles are amenable to analysis by this new reporter strategy.

Minor populations of proteins and protein complexes perform critical functions for the cell. For example, a minor population of the epidermal growth factor receptor present on exosomes mediates intercellular communication¹. A small fraction of the mammalian target of rapamycin, present on lysosomes, is responsible for nutrient sensing by the cell². A minor population of the KDEL receptor present in the Golgi apparatus performs the critical function of retrieving endoplasmic reticulum-resident proteins from the Golgi apparatus³. Small molecules that function as fluorescent reporters of enzymatic activity use highly specific and rapid detection chemistries. However, the cleaved probe molecules diffuse throughout the entire cell and thus location-specific information on protein activity is lost^{4,5}. Alternatively, genetically engineered protein tags provide spatial information^{6,7}, but one can only study the major population of the protein of interest. Thus, it is extremely challenging to selectively address the activity of a minor enzyme population in situ. Here, using DNA nanodevices targeting subcellular organelles we describe a new strategy to exclusively study the activity of a minor population of enzyme in live cells. We demonstrate proof of concept by selectively mapping enzyme-mediated disulfide reduction within endosomes, despite thiol–disulfide exchange occurring rampantly throughout the cell.

Thiol–disulfide exchange occurs mainly in the cytosol, mitochondria and the endoplasmic reticulum to correctly fold disulfide-bridged proteins^{8,9}. Targeted disulfide reduction of specific proteins changes their conformation, thus triggering signalling cascades¹⁰. For example, disulfide reduction of C-terminal SRC kinase results in kinase activation, leading to cell proliferation and cancer¹¹. However, a small proportion of thiol–disulfide exchange occurs in endocytic organelles. Endosomal disulfide reduction is indispensable to degrading endocytosed proteins and pathogenic material as well as for antigen cross-presentation^{12,13}. In fact, several pathogens exploit this chemistry in the endosome to infect host cells¹⁴.

Thiol–disulfide exchange is generally studied using small-molecule probes that are either cell-permeable or do so post endocytosis^{5,15}. Disulfide exchange in the cytosol then enhances probe

fluorescence. While highly specific to thiol–disulfide exchange, such probes cannot report on organellar disulfide exchange. Intra-endosomal disulfide reduction was first established in cell lysates post-treatment with radiolabelled, reducible substrates as probes, analysed as a function of time^{16,17}. However, spatial information is inaccessible to these biochemical methods. While responsive to small thiols such as glutathione (GSH), protein-based redox probes cannot report on enzyme-catalysed disulfide reduction as the disulfide bond in the protein probe is sterically hindered¹⁸.

DNA has proven to be a versatile and engineerable biological scaffold for quantitative imaging in living systems¹⁹. Functional DNA motifs such as aptamers can recognize a range of analytes, and have enabled diverse sensing applications in vitro²⁰. In fact, several detection chemistries have been deployed to ratiometrically image analytes in living systems by leveraging the precise stoichiometry of DNA hybridization to incorporate a reference fluorophore in a well-defined stoichiometry²¹. Molecular trafficking motifs can be integrated on DNA nanodevices to localize them within organelles, enabling chemical mapping^{22,23}. DNA nanodevices attached to diverse endocytic ligands can target specific endocytic pathways¹⁹. We therefore reasoned that by integrating a fluorescent reporter sensitive to thiol–disulfide exchange onto an organelle targetable DNA nanodevice, we would be able to exclusively study endosomal disulfide reduction.

New ratiometric reporters of disulfide exchange

We created a DNA-based, ratiometric reporter consisting of three modules, each with a distinct function (Fig. 1a). The first is a sensing module, consisting of a reaction centre that fluoresces upon thiol–disulfide exchange (Fig. 1a, $\lambda_{em} = 520$ nm). The second comprises a normalizing module, a rhodamine dye (Fig. 1a, $\lambda_{em} = 590$ nm) whose fluorescence properties are redox- and ion-insensitive. The third module comprises a targeting functionality, namely a DNA duplex comprising two oligonucleotides, O-azide and O-Rhodamine Red X (Supplementary Table 1), that serves two purposes. The first is to display the sensing and normalizing modules in a precise, 1:1

¹Department of Chemistry, University of Chicago, Chicago, IL, USA. ²Grossman Institute of Neuroscience, Quantitative Biology and Human Behaviour, University of Chicago, Chicago, IL, USA. *e-mail: yamuna@uchicago.edu

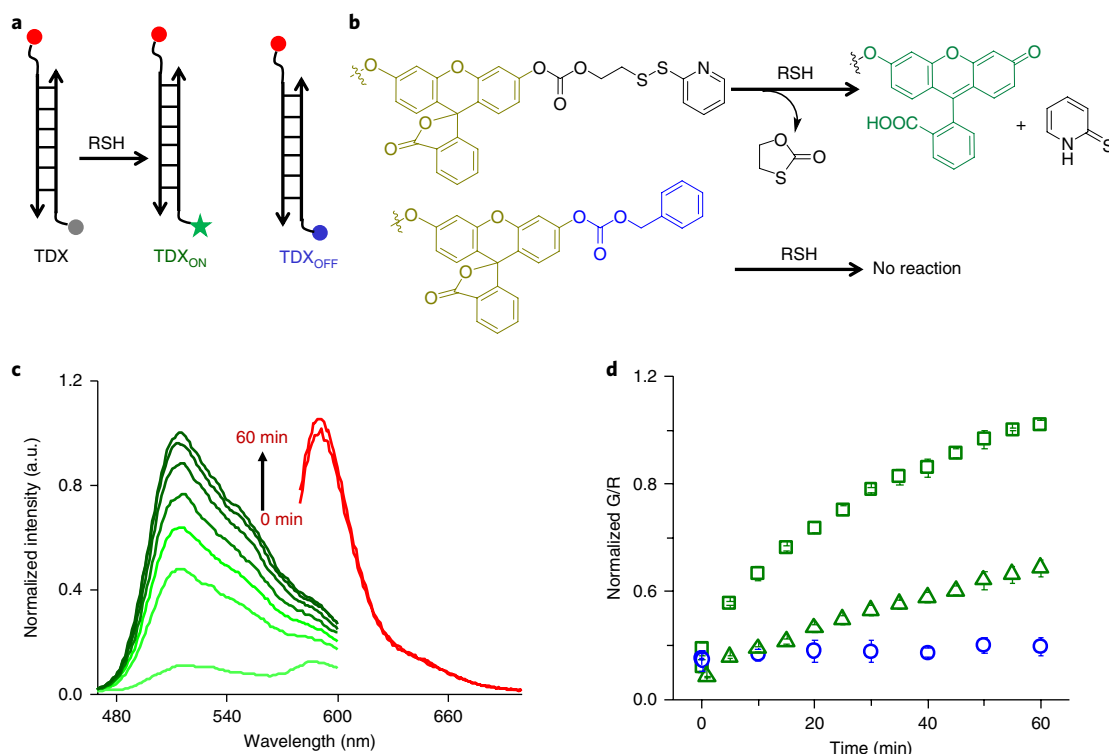


Fig. 1 | Design and in vitro characterization of TDX reporter. **a**, Structure of the TDX (thiol–disulfide exchange) reporter (left): the sensing module (grey) is a caged fluorescein dye conjugated with a disulfide moiety, the normalizing module (red) is a thiol-insensitive rhodamine fluorophore, and the targeting module is a DNA duplex (black lines). The reporter (TDX) undergoes thiol–disulfide exchange to give highly fluorescent TDX_{ON}. TDX_{OFF} (right) is a constitutively off version of TDX where fluorescein is caged by a benzyloxycarbonate group non-responsive to thiols (blue). **b**, Working principle of the sensing module of TDX in the presence of reduced thiols. **c**, Fluorescence emission spectra of the sensing module (green, G) and the normalizing module (red, R) of TDX in 5 mM GSH at pH 7.2 as a function of time. **d**, Ratio of fluorescence intensities (G/R) of TDX_{OFF} (blue open circles, pH 7.2) and TDX in the presence of 5 mM GSH as a function of time at pH 7.2 (green, open squares), pH 6.0 (green, open triangles). Error bars indicate the mean of three independent experiments \pm s.e.m.

stoichiometry. The second is to target the entire assembly to the scavenger receptor-mediated endocytic pathway^{24,25}. All three functions are integrated with stoichiometric precision by hybridizing DNA strands bearing each of these functionalities.

The working principle of the sensing module of the disulfide exchange reporter comprises a fluorescein derivative whose fluorescence is caged using carbonate linker (Fig. 1b)⁴. The other end of the carbonate linker bears a thiopyridyl group via a disulfide bond (Fig. 1b and Supplementary Scheme 1). Disulfide reduction results in deprotection of the fluorescein moiety, leading to high fluorescence at 520 nm.

To make a quantitative reporter system for disulfide reduction suited to the high autofluorescence encountered in vivo, we constructed two more nanodevices. One of these, TDX_{ON}, comprises the DNA duplex attached to fluorescein (Fig. 1a). TDX_{ON} is obtained by completely reducing TDX. As TDX might also turn on due to background hydrolysis of the carbonate linker, we made TDX_{OFF}, in which fluorescein is caged by a non-reducible benzyloxycarbonate moiety (Fig. 1a,b and Supplementary Scheme 2). Thus, TDX_{OFF} reports non-specific hydrolysis and reveals the specificity of disulfide exchange reported by TDX. The syntheses and characterizations of TDX, TDX_{ON} and TDX_{OFF} are described in Supplementary Schemes 1 and 2 and Supplementary Fig. 1a).

In the presence of GSH (5 mM) at pH 7.2, TDX fluorescence at 520 nm (G, fluorescein) increases with time, while the fluorescence of the normalizing module, at 590 nm (R, rhodamine), remains constant (Fig. 1c). Figure 1d shows the G/R ratio of emission intensities as a function of time, which reveals that the reaction is 80%

complete in 30 min. Importantly, under comparable conditions, TDX_{OFF} showed no increase in G/R ratio, indicating that the fluorescence increase observed in TDX is due to disulfide exchange (Fig. 1d and Supplementary Fig. 1b).

TDX detects disulfide exchange in late endosome in vivo

Although genetically encoded redox reporters can be applied to study redox in the cytosol^{18,26}, they cannot be used in organelles due to the acidic luminal pH in organelles. In *Caenorhabditis elegans*, in particular, the glutathione redox potential varies in different tissues and cell types, yet there is no information available at the subcellular level²⁷. We therefore sought to deploy the TDX reporter system to map intra-endosomal thiol–disulfide exchange along the endolysosomal pathway in *C. elegans*.

DNA nanodevices selectively label coelomocytes in *C. elegans* by targeting scavenger receptor-mediated endocytosis^{24,28}. On injection of 2 μ M TDX into the pseudocoelom of wild-type (N2) nematodes, fluorescence images of live worms were acquired in the G and R channels as a function of time. For each time point we constructed ratiometric maps of G/R intensities, represented in pseudocolour (Methods and Fig. 2a). We observed that the G/R ratio was maximal at 20 min post injection and remained almost constant thereafter (Fig. 2a,b). A similar experiment using TDX_{OFF} gave a G/R ratio that remained unchanged (Fig. 2b and Supplementary Fig. 2). This indicates that the increase in G/R ratio shown by TDX is due to thiol–disulfide exchange and not from esterolysis.

The tripartite reporter comprising TDX_{ON}, TDX_{OFF} and TDX jointly corrects for any pH effects on the fluorescence of the sensor

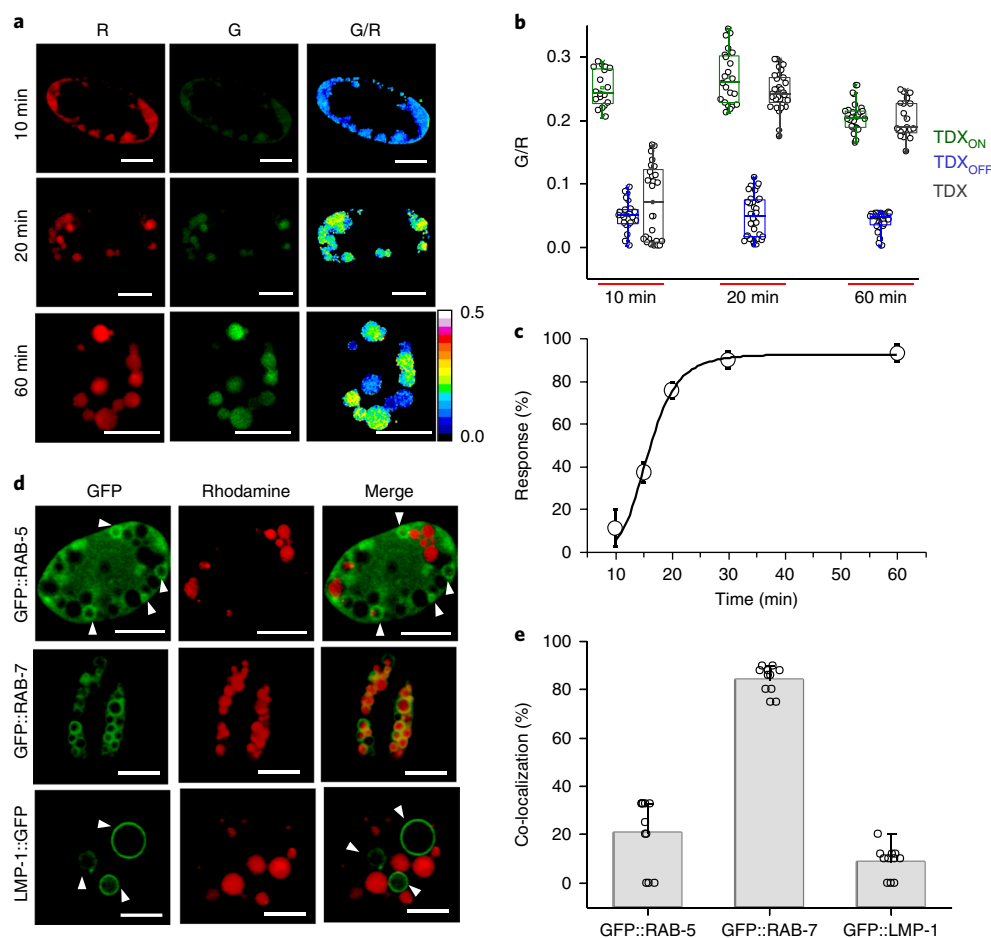


Fig. 2 | Spatiotemporal detection of the thiol-disulfide exchange reaction in the endo-lysosomal compartment of *C. elegans* coelomocytes.

a, Representative pseudo-coloured images of TDX reporter endocytosis by coelomocytes at the indicated time points post injection. **b**, Box plot showing G/R ratio at different time points ($n=20$ cells, ≥ 80 endosomes). Circles represent mean G/R value of coelomocytes. Box represents the upper and lower quartiles of the G/R distribution. Horizontal solid line in the middle of the box represents the median value. Whiskers represent the variability of G/R value outside the upper and lower quartiles. **c**, Plot of percentage response of TDX reporter at different time points post injection in worms, Error bars, Mean of three independent experiments \pm s.e.m. **d**, Co-localization of TDX^R with transgenic worms expressing molecular markers of endocytic vesicles such as GFP::RAB-5, GFP::RAB-7 and LMP-1::GFP in coelomocytes, 20 min post injection ($n=10$ cells, ≥ 50 endosomes). Scale bars, 5 μ m. **e**, Quantification of co-localization in **d**.

module. For example, the luminal pH decreases along the endocytic pathway, which could affect the fluorescein intensity. We correct for this by performing three sets of experiments at each time point, injecting either TDX_{ON}, TDX_{OFF} or TDX, obtaining G and R images, heat maps and G/R values (Fig. 2b). We calculated the percentage response of TDX (Fig. 2c) as a function of time using equation (1) (Methods). This yielded a sigmoidal curve for thiol-disulfide exchange as a function of time; 20 min post injection the reaction was complete (Fig. 2c).

For the first 10 min, the TDX response is negligible, and then starts reacting at $t=15$ min; by $t=20$ min the reaction is $\sim 80\%$ complete. Co-localization studies with endosomal markers in transgenic nematodes were performed. Rhodamine-labelled dsDNA, denoted TDX^R, was injected in nematodes expressing GFP::RAB-5 as an early endosomal marker, GFP::RAB-7 as a late endosomal/lysosomal marker and LMP-1::GFP as a lysosomal marker (Fig. 2d). At $t=20$ min post injection, TDX^R showed 85% co-localization with GFP::RAB-7 (Fig. 2e), indicating its localization in late endosomes. This reveals that thiol-disulfide exchange occurs in late endosomes in coelomocytes.

The observed intra-endosomal disulfide exchange could be mediated by small molecules such as cysteine, GSH and H₂S, or by

enzymes^{16,29}. Using a well-characterized, icosahedral DNA nanocapsule reporter system (Supplementary Figs. 3 and 4)^{30,31}, we found that uncatalysed thiol-disulfide exchange mediated by small biologically available thiols was negligible.

PDI-3 and TRX-1 catalyse thiol exchange in late endosomes

Next, we sought to identify the protein players, if any, that mediated intra-endosomal disulfide reduction in coelomocytes. Proteins that catalyse disulfide exchange generally contain thioredoxin domains, for example thioredoxins or protein disulfide isomerases³². Using BLASTP³³ we found approximately 23 proteins in the *C. elegans* genome that contained at least one thioredoxin domain (Supplementary Fig. 16). We excluded seven that contained either mitochondrial or nuclear localization sequences, which precluded their endosomal localization (Supplementary Table 2). We then knocked down each of the 15 candidate genes by RNA interference (RNAi) and, in each genetic background, we quantitated the percentage response of the TDX reporter due to intra-endosomal thiol-disulfide exchange (Fig. 3b). We obtained two clear hits, where knocking down *pdi-3* or *trx-1* showed 50% and 40% reduction in disulfide exchange respectively as compared to wild type

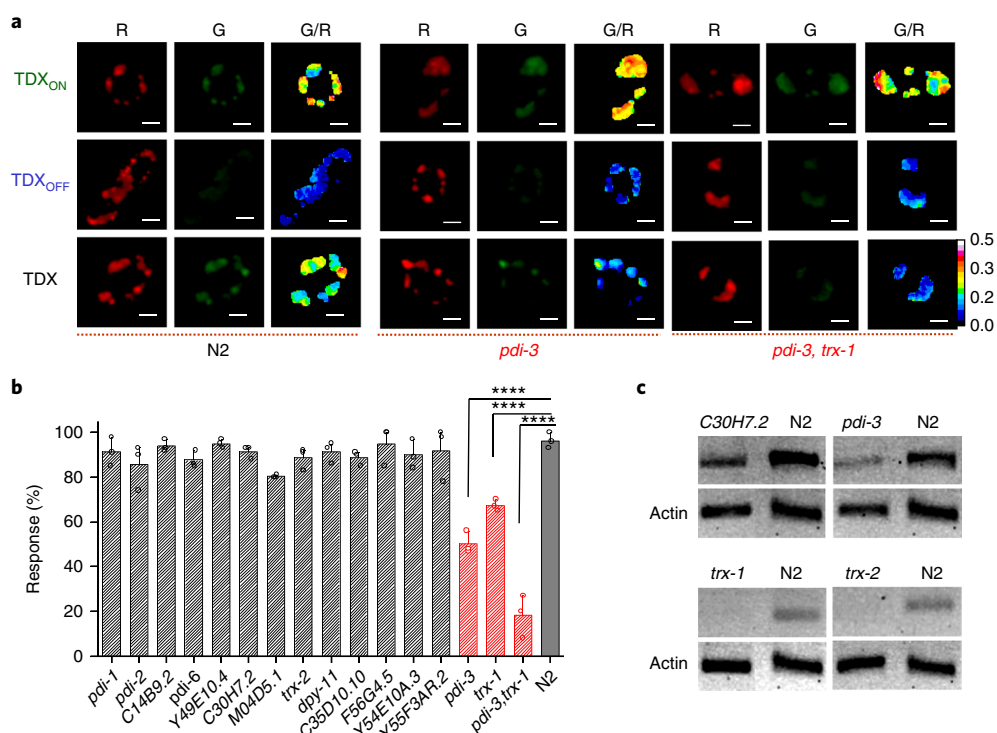


Fig. 3 | PDI-3 and TRX-1 are responsible for the disulfide exchange reaction inside endocytic vesicles. a, Representative pseudo-colour images of coelomocytes labelled individually with TDX_{ON}, TDX_{OFF} and TDX in worms of the indicated genetic backgrounds. **b**, Plot of % response of TDX in different mutants and RNAi knockdowns 20 min post injection. Error bars indicate the mean of three independent experiments \pm s.e.m. ($n=10$ cells, ≥ 50 endosomes). ****Two-tailed $P < 0.0001$ in unpaired t -test, % response of *pdi-3*, *trx-1* and *pdi-3;trx-1* double RNAi worms at 20 min post injection. **c**, RT-PCR analysis of total RNA isolated from wild-type (N2) and RNAi worms. PCR amplified cDNA of specified gene products in both RNAi and N2 worms are shown. Actin is used as a loading control. Scale bars, 5 μ m.

nematodes (Fig. 3b). Simultaneous knockdown of both *pdi-3* and *trx-1* in nematodes showed a dramatic reduction of disulfide exchange, nearly comparable to G/R values seen with TDX_{OFF} (Fig. 3a). This indicates that disulfide reduction in the late endosome is predominantly due to *pdi-3* and *trx-1*. The efficiency of RNAi knockdown of relevant genes were confirmed by RT-PCR followed by gel electrophoresis (Fig. 3c).

TRX-1 mainly reduces several disulfide-containing proteins, and thereby serves to enhance the activity of stronger reducing proteins, such as the protein disulfide isomerases (PDIs). In fact, the oxidation potential of PDIs is nearly 50-fold higher than that of thioredoxin³⁴, suggesting that PDI-3 could also function along with TRX-1 at the acidic pH in the late endosome²⁴. Thioredoxin-1 (TRX-1) is maximally present in the cytosol, while PDI-3 is maximally present in the endoplasmic reticulum due to its strong endoplasmic reticulum retention signal³⁵. It is notable that, despite the presence of PDI-3 and TRX-1 on the plasma membrane, as well as 1–10 μ M extracellular GSH³⁶, our nanodevice reporters are reduced specifically in the late endosome. This reveals the existence of a minor, catalytically active pool of PDI-3 and TRX-1 in the late endosome where they bring about intra-endosomal disulfide exchange.

Endosomal disulfide exchange assists pathogen infection

Disulfide exchange is co-opted by pathogens like *Burkholderia cenocapacia*, *Corynebacterium diphtheriae*, the HIV virus, the rotavirus ECwt, Ganjam virus and so on, so that they can efficiently infect host cells^{37–41}. We addressed the significance of the catalytic activities of our hits PDI-3 and TRX-1 in endosomes by investigating their roles in mediating pathogen infection. For this, we used a previously established *C. diphtheriae* infection model in *C. elegans*⁴¹.

Briefly, *C. diphtheriae* secretes an AB toxin called diphtheria toxin (DT), comprising a non-toxic B-subunit (DT-B) and a toxic A-subunit (DT-A) linked through a disulfide bond. This bond is reduced within the endosomes and DT-A thereby translocates into the cytosol, inhibiting protein synthesis in the host cell. Disulfide reduction is thus a critical step to bring about toxin infection (Supplementary Fig. 8).

We used the transgenic nematode *cl2070*, which expresses green fluorescent protein (GFP) under a heat shock promoter *hsp-16.2* in all tissues. Successful infection by *C. diphtheriae* is expected to result in cytosolic DT-A compromising protein synthesis leading to nematodes that fail to express GFP in the pharynx upon heat shock⁴². Accordingly, nematodes infected with *C. diphtheriae* showed significantly less GFP in the pharynx as compared to non-infected nematodes (Fig. 4a). Notably, GFP intensity in the gut was comparable in both infected and non-infected nematodes as the site of action of *C. diphtheriae* is not the gut, but the pharynx (Fig. 4b,c and Supplementary Figs. 6 and 7)⁴¹.

Next, we examined the consequences of inhibiting intra-endosomal disulfide reduction on diphtheria toxin infection by knocking down *pdi-3* and/or *trx-1* in this infection model. We observed that *trx-1*, but not *pdi-3*, knockdowns show retention of pharyngeal GFP expression on treatment with *C. diphtheriae* (Fig. 4a,b). This indicates that by knocking down endosomal disulfide exchange brought about by the minor endosomal population of thioredoxin-1 impedes diphtheria toxin infection by reducing the cytosolic translocation of DT-A. Knocking down both *pdi-3* and *trx-1* also prevents diphtheria toxin infection (Fig. 4b). In coelomocytes, we observe that PDI-3 and TRX-1 are both involved in endosomal disulfide reduction but in the case of diphtheria toxin infection

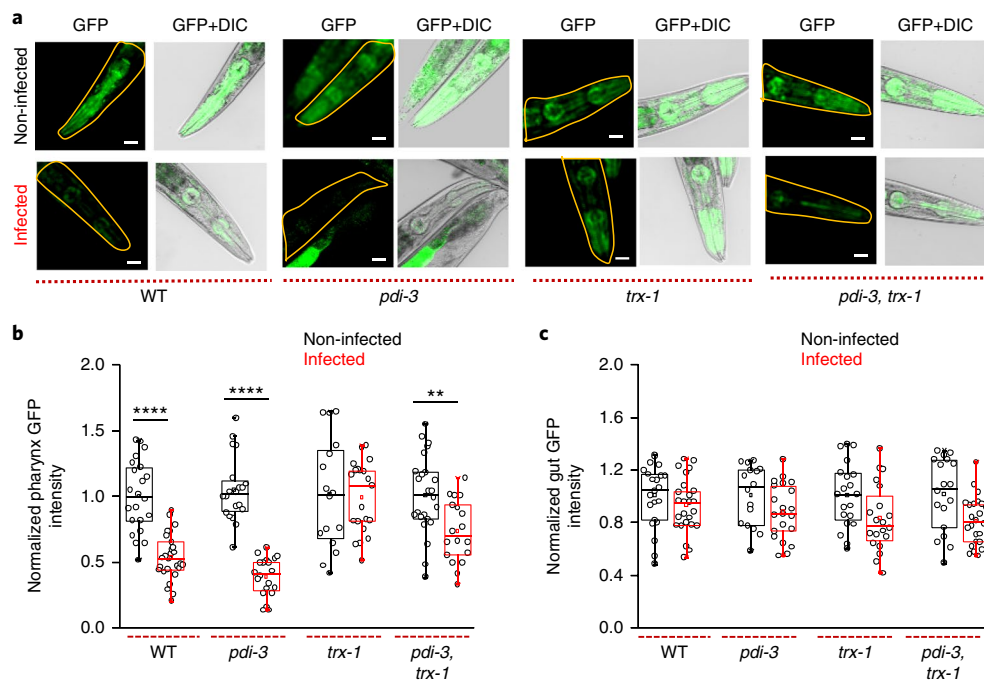


Fig. 4 | Thioredoxin-1 offers protection against diphtheria toxin infection. **a**, Representative pseudo-colour and overlaid images of pharyngeal GFP expression in indicated genetic backgrounds of nematodes infected or not infected with *C. diphtheriae*. Box plots of normalized pharyngeal (**b**) and intestinal (**c**) GFP intensity of infected and non-infected nematodes with indicated genetic background ($n=20$ worms). GFP intensity distribution is normalized by the mean intensity of the respective not-infected worm. **** $P < 0.0001$, ** $P < 0.005$, obtained using unpaired *t*-test. Scale bars, 100 μm . Experiments were replicated in duplicate.

only TRX-1 is responsible. Even though both TRX-1 and PDI-3 were responsible for intra-endosomal disulfide reduction, we found that diphtheria toxin infection depends on the minor pool of TRX-1, and not PDI-3. This is also consistent with *in vitro* studies that show that the intra-chain disulfide bond of diphtheria toxin is a good substrate for thioredoxin-1 at acidic pH⁴³. Our findings reveal that diphtheria toxin exploits intra-endosomal reduction by thioredoxin-1 *in vivo* and that inhibiting this minor pool impedes diphtheria toxin infection.

TRX-1 mediates endosomal disulfide exchange in human cells

Next, we sought to generalize this reporter technology by probing disulfide reduction in a mammalian cell culture system. All TDX reporters undergo scavenger receptor-mediated endocytosis in HeLa cells on incubation with 1 μM of any TDX reporter⁴⁴. We could therefore follow disulfide reduction as a function of time using TDX reporters as described (Supplementary Fig. 11). While we observed no disulfide reduction for the first 2 h, TDX reporters started responding at $t=3$ h and the reaction was complete by $t=4$ h (Fig. 5a,b). The analogous experiment with TDX_{OFF} showed negligible change in G/R ratio (Fig. 5a). We pharmacologically inhibited disulfide isomerases in HeLa cells using *N*-ethyl maleimide (NEM) or by blocking surface and endosomal thiols using 5,5'-dithio-bis-(2-nitrobenzoic acid) (DTNB). Both treatments reduced the reporter response by ~90%, confirming that endosomal disulfide reduction was indeed responsible for the signal increase (Fig. 5d and Supplementary Fig. 12).

Co-localization studies with various endosomal markers indicated that the observed disulfide reduction occurred in the late endosome. We pulsed HeLa cells expressing Rab5-RFP as an early endosomal marker or Rab7-RFP as a late endosomal marker with TDX bearing a single Alexa-647 fluorophore (TDX^{A647}) and assayed for co-localization after a 3 h chase. We observed ~70% co-localization

with Rab7-RFP and insignificant co-localization with Rab5-GFP. Lysosomes were labelled with TMR-dextran through fluid phase endocytosis after a 1 h pulse and 12 h chase. HeLa cells pre-labelled thus were then pulsed and chased with TDX^{A647} as above and showed negligible co-localization with lysosomes (Fig. 5c).

To identify the major protein player involved in this reduction, we knocked down the human analogues of PDI-3 and TRX-1 by RNAi. HeLa cells where Erp57 and TRX-1 were each knocked down were investigated using the tripartite reporter system and the G/R ratios were obtained. We observed that disulfide reduction in TRX-1 depleted cells was reduced by >70% compared to normal cells, while Erp57 depleted cells showed negligible change (Fig. 5d and Supplementary Fig. 12). This indicates that, in mammalian cells, a minor pool of endosomal resident TRX-1 plays a major role in endosomal disulfide reduction.

Summary

The modular design of our DNA-based tripartite fluorescent reporter system enables quantitative imaging of intra-endosomal disulfide exchange *in situ* in coelomocytes of *C. elegans* as well as in mammalian cells. It revealed that thiol–disulfide exchange along the endolysosomal pathway occurs mainly in the late endosome. We ruled out small-molecule thiol-mediated reduction in late endosomes, implicating the action of proteins in these acidic compartments. In fact, the pK_a of the N-terminal active site cysteine of PDI can be as low as 4.8, while that of thioredoxins can range between ~6.0 and 7.0 (ref. 45). This is in consistent with the rapid thiol reduction kinetics we observe in the acidic late endosome lumen, supporting that disulfide exchange is likely to be enzyme-catalysed.

Quantitative imaging of thiol–disulfide exchange in RNAi knockdowns of various candidate genes revealed that PDI-3 and TRX-1 were the enzymes responsible for the observed intra-endosomal disulfide reduction *in vivo*. Although PDI-3 and TRX-1 are

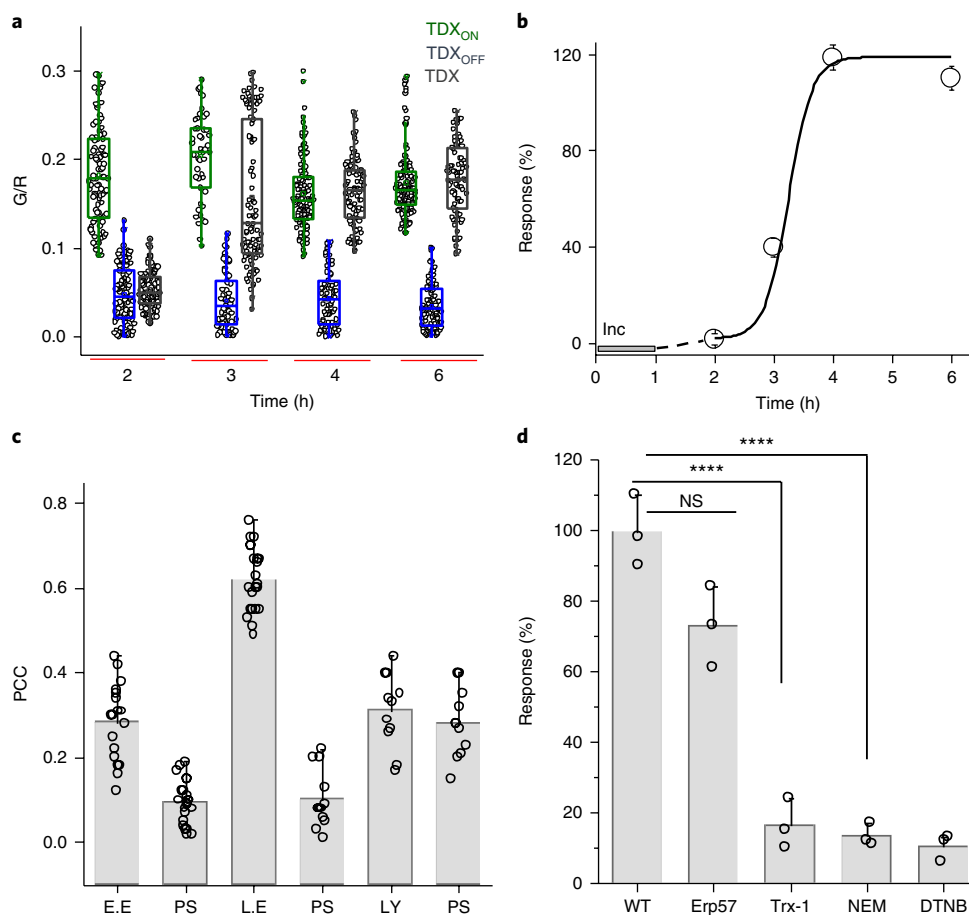


Fig. 5 | TRX-1 mediates endosomal disulfide reduction in mammalian cells. **a**, Box plot of G/R values of the TDX reporter system in HeLa cells at the indicated time points post internalization ($n = 20$ cells, ≥ 150 endosomes). **b**, Percentage response of the TDX reporter system as a function of time (Inc., incubation period; line serves as a visual aid). **c**, Pearson's correlation coefficient (PCC) of co-localization between pulsed TDXA647 after a 3 h chase in HeLa cells expressing endosomal markers. (EE, early endosome, Rab5-RFP; LE, late endosome, Rab7-RFP; Ly, lysosome, TMR dextran; PS, pixel shift) ($n \geq 10$ cells). **d**, Percentage response of the TDX reporter system at $t = 4$ h in HeLa cells treated with indicated inhibitors or siRNAs against indicated proteins (NEM, *N*-ethyl maleimide; DTNB, 5, 5-dithio-bis-(2-nitrobenzoic acid)). Error bars, S.e.m. from three independent experiment; NS, not significant; **** $P < 0.0001$; obtained using unpaired *t*-test.

predominantly localized in the endoplasmic reticulum and cytosol, respectively^{35,46}, a minor pool of these proteins is localized in subcellular compartments where they perform critical functions. Using a diphtheria toxin infection model, we found that inhibiting the catalytic activity of this minor population of enzyme inside the endosome protects the host cell from pathogen infection. The reporter system revealed that TRX-1 was also responsible for disulfide reduction in late endosomes of human cells. Given the large number of toxins and pathogens that exploit intra-endosomal disulfide reduction to bring about infection⁴⁰, our work suggests that the selective inhibition of intra-endosomal disulfide exchange could be of interest to develop anti-infectives.

The advantage of this tripartite reporter system is the newfound ability to directly and selectively assay, in live cells and with spatial information, the enzyme activity of protein populations in organelles by localizing the detection chemistry within the organelle (Supplementary Figs. 14 and 15). The stoichiometric precision of DNA hybridization enables two major advantages, unique to DNA-based probes and inaccessible to any other reporter technology: (1) molecularly identical probes with fixed, uniform sensor-to-normalizer ratios that quantify a given analyte with accuracies unmatched by any other molecular scaffold; (2) 'plug-and-play' capability due to its modular nature (once a DNA probe is validated,

it can be directly used in a host of other organelle locations by simply swapping out one organelle targeting module for any other)^{47,48}.

It can thus be readily integrated with the existing diversity of small-molecule reporters and enzyme-cleavage chemistries to provide robust readouts exclusively in organelles in situ within living cells (Supplementary Table 3). For example, lysosomal enzyme chemistries may be integrated to measure lysosomal enzyme activity in situ, with applications in lysosomal storage disorders⁴⁹. The catalytic activity of endosomal proteases such as cathepsin B, cathepsin D or β -secretase-1 results in protein processing events leading to cancer and Alzheimer's disease^{50,51}. Protease action by pro-protein convertases in the Golgi underlie neurogenesis, TGF- β signalling and A β_3 toxin infection⁵². The ability of DNA nanodevices to selectively quantitate subcellular enzymatic cleavage in live cells could provide new diagnostics and drug discovery assays.

This new system can also be integrated with newer reporting strategies that probe enzymatic function such as activity-based protein probes to identify enzymatic activity in cellular compartments⁵³. The advent of transformative technologies such as fluorescent proteins, SNAP-tag⁵⁴ or Halo-tag⁷ ushered in a new era of visualizing proteins⁶ in situ by enabling methods to image the major population of any protein of interest. The organelle-targetable nanodevice system described here effectively complements these

powerful technologies by selectively interrogating minor populations of enzymes involved in critical cellular functions, which cannot otherwise be studied.

Online content

Any methods, additional references, Nature Research reporting summaries, source data, statements of data availability and associated accession codes are available at <https://doi.org/10.1038/s41565-019-0365-6>.

Received: 15 September 2017; Accepted: 18 December 2018;

Published online: 11 February 2019

References

- Huang, S.-H., Li, Y., Zhang, J., Rong, J. & Ye, S. Epidermal growth factor receptor-containing exosomes induce tumor-specific regulatory T cells. *Cancer Invest.* **31**, 330–335 (2013).
- Efeyan, A., Comb, W. C. & Sabatini, D. M. Nutrient-sensing mechanisms and pathways. *Nature* **517**, 302–310 (2015).
- Dean, N. & Pelham, H. R. Recycling of proteins from the Golgi compartment to the ER in yeast. *J. Cell Biol.* **111**, 369–377 (1990).
- Bhuniya, S. et al. An activatable theranostic for targeted cancer therapy and imaging. *Angew. Chem. Int. Ed.* **53**, 4469–4474 (2014).
- Lee, M. H. et al. Hepatocyte-targeting single galactose-appended naphthalimide: a tool for intracellular thiol imaging in vivo. *J. Am. Chem. Soc.* **134**, 1316–1322 (2012).
- Crivat, G. & Taraska, J. W. Imaging proteins inside cells with fluorescent tags. *Trends Biotechnol.* **30**, 8–16 (2012).
- Los, G. V. et al. HaloTag: a novel protein labeling technology for cell imaging and protein analysis. *ACS Chem. Biol.* **3**, 373–382 (2008).
- Gething, M. J. & Sambrook, J. Protein folding in the cell. *Nature* **355**, 33–45 (1992).
- Mesecke, N. et al. A disulfide relay system in the intermembrane space of mitochondria that mediates protein import. *Cell* **121**, 1059–1069 (2005).
- Burgoyne, J. R. et al. Cysteine redox sensor in PKGI α enables oxidant-induced activation. *Science* **317**, 1393–1397 (2007).
- Mills, J. E. et al. A novel disulfide bond in the SH2 domain of the C-terminal Src kinase controls catalytic activity. *J. Mol. Biol.* **365**, 1460–1468 (2007).
- Collins, D. S., Unanue, E. R. & Harding, C. V. Reduction of disulfide bonds within lysosomes is a key step in antigen processing. *J. Immunol.* **147**, 4054–4059 (1991).
- Guermonez, P. et al. ER-phagosome fusion defines an MHC class I cross-presentation compartment in dendritic cells. *Nature* **425**, 397–402 (2003).
- Stolf, B. S. et al. Protein disulfide isomerase and host–pathogen interaction. *ScientificWorldJournal* **11**, 1749–1761 (2011).
- Maiti, S. et al. Gemcitabine–coumarin–biotin conjugates: a target specific theranostic anticancer prodrug. *J. Am. Chem. Soc.* **135**, 4567–4572 (2013).
- Feener, S. E., Shene, W.-C. & Ryser, H. Cleavage of disulfide bonds in endocytosed macromolecules. *J. Biol. Chem.* **265**, 18780–18785 (1990).
- Shen, W. C., Ryser, H. J. & LaManna, L. Disulfide spacer between methotrexate and poly(D-lysine). A probe for exploring the reductive process in endocytosis. *J. Biol. Chem.* **260**, 10905–10908 (1985).
- Meyer, A. J. & Dick, T. P. Fluorescent protein-based redox probes. *Antioxid. Redox Signal.* **13**, 621–650 (2010).
- Chakraborty, K., Veetil, A. T., Jaffrey, S. R. & Krishnan, Y. Nucleic acid-based nanodevices in biological imaging. *Annu. Rev. Biochem.* **85**, 349–373 (2016).
- Liu, J., Cao, Z. & Lu, Y. Functional nucleic acid sensors. *Chem. Rev.* **109**, 1948–1998 (2009).
- Modi, S. et al. A DNA nanomachine that maps spatial and temporal pH changes inside living cells. *Nat. Nanotechnol.* **4**, 325–330 (2009).
- Modi, S., Nizak, C., Surana, S., Halder, S. & Krishnan, Y. Two DNA nanomachines map pH changes along intersecting endocytic pathways inside the same cell. *Nat. Nanotechnol.* **8**, 459–467 (2013).
- Saha, S., Prakash, V., Halder, S., Chakraborty, K. & Krishnan, Y. A pH-independent DNA nanodevice for quantifying chloride transport in organelles of living cells. *Nat. Nanotechnol.* **10**, 645–651 (2015).
- Surana, S., Bhat, J. M., Koushika, S. P. & Krishnan, Y. An autonomous DNA nanomachine maps spatiotemporal pH changes in a multicellular living organism. *Nat. Commun.* **2**, 340 (2011).
- Narayanaswamy, N. et al. A pH-correctable, DNA-based fluorescent reporter for organellar calcium. *Nat. Methods* **16**, 95–102 (2019).
- Gutscher, M. et al. Real-time imaging of the intracellular glutathione redox potential. *Nat. Methods* **5**, 553–559 (2008).
- Romero-Aristizabal, C., Marks, D. S., Fontana, W. & Apfeld, J. Regulated spatial organization and sensitivity of cytosolic protein oxidation in *Caenorhabditis elegans*. *Nat. Commun.* **5**, 5020 (2014).
- Chakraborty, K., Leung, K. & Krishnan, Y. High luminal chloride in the lysosome is critical for lysosome function. *eLife* **6**, e28862 (2017).
- Yang, J., Chen, H., Vlahov, I. R., Cheng, J.-X. & Low, P. S. Evaluation of disulfide reduction during receptor-mediated endocytosis by using FRET imaging. *Proc. Natl Acad. Sci. USA* **103**, 13872–13877 (2006).
- Bhatia, D. et al. Icosahedral DNA nanocapsules by modular assembly. *Angew. Chem. Int. Ed.* **48**, 4134–4137 (2009).
- Veetil, A. T., Jani, M. S. & Krishnan, Y. Chemical control over membrane-initiated steroid signaling with a DNA nanocapsule. *Proc. Natl Acad. Sci. USA* **115**, 9432–9437 (2018).
- Sevier, C. S. & Kaiser, C. A. Formation and transfer of disulphide bonds in living cells. *Nat. Rev. Mol. Cell Biol.* **3**, 836–847 (2002).
- Altschul, S. F., Gish, W., Miller, W., Myers, E. W. & Lipman, D. J. Basic local alignment search tool. *J. Mol. Biol.* **215**, 403–410 (1990).
- Hawkins, H. C., Blackburn, E. C. & Freedman, R. B. Comparison of the activities of protein disulphide-isomerase and thioredoxin in catalysing disulphide isomerization in a protein substrate. *Biochem. J.* **275**, 349–353 (1991).
- Eschenlauer, S. C. P. & Page, A. P. The *Caenorhabditis elegans* ERp60 homolog protein disulfide isomerase-3 has disulfide isomerase and transglutaminase-like cross-linking activity and is involved in the maintenance of body morphology. *J. Biol. Chem.* **278**, 4227–4237 (2003).
- Smith, C. V., Jones, D. P., Guenther, T. M., Lash, L. H. & Lauterburg, B. H. Compartmentation of glutathione: implications for the study of toxicity and disease. *Toxicol. Appl. Pharmacol.* **140**, 1–12 (1996).
- Rubartelli, A., Bajetto, A., Allavena, G., Wollman, E. & Sitia, R. Secretion of thioredoxin by normal and neoplastic cells through a leaderless secretory pathway. *J. Biol. Chem.* **267**, 24161–24164 (1992).
- Dihazi, H. et al. Secretion of ERP57 is important for extracellular matrix accumulation and progression of renal fibrosis, and is an early sign of disease onset. *J. Cell Sci.* **126**, 3649–3663 (2013).
- Pacello, F., D’Orazio, M. & Battistoni, A. An ERp57-mediated disulphide exchange promotes the interaction between *Burkholderia cenocepacia* and epithelial respiratory cells. *Sci. Rep.* **6**, 21140 (2016).
- Lasecka, L. & Baron, M. D. Theairovirus nairobi sheep disease virus/ganjam virus induces the translocation of protein disulfide isomerase-like oxidoreductases from the endoplasmic reticulum to the cell surface and the extracellular space. *PLoS One* **9**, e94656 (2014).
- Ott, L. et al. Evaluation of invertebrate infection models for pathogenic corynebacteria. *FEMS Immunol. Med. Microbiol.* **65**, 413–421 (2012).
- Dunbar, T. L., Yan, Z., Balla, K. M., Smelkinson, M. G. & Troemel, E. R. *C. elegans* detects pathogen-induced translational inhibition to activate immune signaling. *Cell Host Microbe* **11**, 375–386 (2012).
- Moskaug, J. O., Sandvig, K. & Olsnes, S. Cell-mediated reduction of the interfragment disulfide in nicked diphtheria toxin. A new system to study toxin entry at low pH. *J. Biol. Chem.* **262**, 10339–10345 (1987).
- Patel, P. C. et al. Scavenger receptors mediate cellular uptake of polyvalent oligonucleotide-functionalized gold nanoparticles. *Bioconjug. Chem.* **21**, 2250–2256 (2010).
- Karala, A.-R., Lappi, A.-K. & Ruddock, L. W. Modulation of an active-site cysteine pKa allows PDI to act as a catalyst of both disulfide bond formation and isomerization. *J. Mol. Biol.* **396**, 883–892 (2010).
- Wu, C. et al. Thioredoxin 1-mediated post-translational modifications: reduction, transnitrosylation, denitrosylation, and related proteomics methodologies. *Antioxid. Redox Signal.* **15**, 2565–2604 (2011).
- Thekkan, S. et al. A DNA-based fluorescent reporter maps HOCl production in the maturing phagosome. *Nat. Chem. Biol.* <https://doi.org/10.1038/s41589-018-0176-3> (2018).
- Leung, K., Chakraborty, K., Saminathan, A. & Krishnan, Y. A DNA nanomachine chemically resolves lysosomes in live cells. *Nat. Nanotechnol.* <https://doi.org/10.1038/s41565-018-0318-5> (2018).
- Futerman, A. H. & van Meer, G. The cell biology of lysosomal storage disorders. *Nat. Rev. Mol. Cell Biol.* **5**, 554–565 (2004).
- Olson, O. C. & Joyce, J. A. Cysteine cathepsin proteases: regulators of cancer progression and therapeutic response. *Nat. Rev. Cancer* **15**, 712–729 (2015).
- Vassar, R., Kovacs, D. M., Yan, R. & Wong, P. C. The beta-secretase enzyme BACE in health and Alzheimer’s disease: regulation, cell biology, function, and therapeutic potential. *J. Neurosci.* **29**, 12787–12794 (2009).
- Seidah, N. G. & Prat, A. The biology and therapeutic targeting of the proprotein convertases. *Nat. Rev. Drug Discov.* **11**, 367–383 (2012).
- Nomura, D. K., Dix, M. M. & Cravatt, B. F. Activity-based protein profiling for biochemical pathway discovery in cancer. *Nat. Rev. Cancer* **10**, 630–638 (2010).
- Prifti, E. et al. A fluorogenic probe for SNAP-tagged plasma membrane proteins based on the solvatochromic molecule Nile Red. *ACS Chem. Biol.* **9**, 606–612 (2014).

Acknowledgements

The authors thank J. Clardy, J. Kuriyan, S. Modi and A. Lin Chun for valuable comments on this work. The authors thank the Integrated Light Microscopy facility at the University of Chicago, the *Caenorhabditis* Genetic Center (CGC), J. Fares and M. Edgley for *C. elegans* strains, M. Glotzer and F. M. Ausubel for RNAi clones and valuable discussions, S. Crosson at the BSL facility for *C. diphtheriae* work and C. Cui for BMDMs and flow cytometry. This work was supported by the University of Chicago Women's Board, Chicago Biomedical Consortium with support from the Searle Funds at The Chicago Community Trust, C-084 as well as a CBC post-doctoral research grant (PDR-073), Pilot and Feasibility award from an NIDDK Center grant P30DK42086 to the University of Chicago Digestive Diseases Research Core Center and University of Chicago start-up funds to Y.K. Y.K. is a Brain Research Foundation Fellow.

Author contributions

K.D. and Y.K. designed the project. K.D. developed tripartite TDX reporters and performed all experiments related to TDX reporter in *C. elegans* and mammalian cells. A.T.V. prepared the dextran encapsulated icosahedron and in vitro experiments related

to icosahedron. K.C. contributed to cathepsin-related experiments. K.D., A.T.V., K.C. and Y.K. analysed the data. K.D., A.T.V. and Y.K. wrote the paper. All authors discussed the results and provided input on the manuscript.

Competing interests

The authors declare no competing interests.

Additional information

Supplementary information is available for this paper at <https://doi.org/10.1038/s41565-019-0365-6>.

Reprints and permissions information is available at www.nature.com/reprints.

Correspondence and requests for materials should be addressed to Y.K.

Publisher's note: Springer Nature remains neutral with regard to jurisdictional claims in published maps and institutional affiliations.

© The Author(s), under exclusive licence to Springer Nature Limited 2019

Methods

Materials and methods. All the chemicals used for the synthesis were purchased from Sigma. ^1H NMR and ^{13}C NMR spectra of the newly synthesized compounds were recorded on a Bruker AVANCE II+, 500 MHz NMR spectrophotometer. Tetramethylsilane (TMS) was used as an internal standard. Mass spectra were recorded with an Agilent 6224 Accurate-Mass time-of-flight (TOF) liquid chromatography–mass spectrometry (LC/MS). High performance liquid chromatography (HPLC)-purified oligonucleotides conjugated with either fluorophore or azide functional group were obtained from Integrated DNA Technologies. All oligonucleotides were ethanol-precipitated and quantified by UV absorbance at $\lambda = 260$ nm.

Synthesis of TDX reporter. Rhodamine- and azide-labelled DNA-strand (O-Rhodamine Red X and O-azide) (Supplementary Table 1) were mixed in an equimolar concentration (25 μM each) in 20 mM phosphate buffer containing 100 mM KCl at pH 7. The mixture was heated at 90 °C for 10 min and then cooled to room temperature at a rate of 5 °C per 15 min and stored at 4 °C overnight to form a complete DNA-duplex.

Rhodamine–DNA-duplex was then conjugated with the thiol-sensitive fluorescein derivative (compound 8, Supplementary Scheme 1), by a copper-catalysed azide-alkyne click chemistry protocol⁶⁵. Initially 20 μl rhodamine-conjugated DNA duplex was (25 μM) diluted in 13.5 μl water, to which 3 μl of compound 8 (5 mM) in DMSO was added. A 1:1 (vol/vol) premix solution of 7.5 μl of CuSO_4 (0.1 M) and tris-hydroxypropyltriazolylmethylamine (THPTA) (0.2 M) was then added. The reaction mixture was degassed with N_2 for 2 min and 6 μl of sodium ascorbate (0.1 M) was added. The mixture was further degassed for 0.5 min and then stirred at room temperature for 1 h under a N_2 atmosphere. Native PAGE (20 wt%) showed complete formation of TDX reporter (Fig. 1a and Supplementary Fig. 1a). Subsequently, the reaction mixture was diluted with pH 6.0 phosphate buffer and washed with 10% acetonitrile (to remove excess compound 8 using an Amicon Ultra-0.5 ml centrifugal filter, molecular weight cutoff (MWCO) of 3 kDa). The same washing procedure was continued until the filtrate showed no trace of compound 8 using fluorescence spectroscopy ($\lambda_{\text{em}} = 520$ nm). Native gel electrophoresis was then performed and monitored by fluorescence, which revealed negligible single strands in our preparations.

Synthesis of TDX_{ON} reporter. TDX reporter (10 μl , 8 μM) was mixed with 1 μl (5 mM) NaSH solution in 0.1 M phosphate buffer at pH 7.4 and stirred for 2 h at room temperature. Excess thiol was then removed by ultracentrifugation using an Amicon filter (MWCO, 3 kDa) to obtain TDX_{ON} reporter (Fig. 1a).

Synthesis of TDX_{OFF} reporter. TDX_{OFF} reporter was prepared in a procedure similar to that used for the TDX reporter, except that compound 9 (the thiol-insensitive fluorescein derivative, Supplementary Scheme 2) was used instead of compound 8. The formation of TDX_{OFF} reporter was characterized using gel electrophoresis (Supplementary Fig. 1a).

Conjugation of compound 8 with azido dextran. Azido functionalized dextran (2 mg, 10 kDa, two to three azido groups per dextran) was dissolved in 90 μl milliQ water. Compound 8 (20 μl , 5 mM), followed by 50 μl CuSO_4 (0.1 M) and THPTA (0.2 M) mixture (1:1), was added. The reaction mixture was degassed for 2 min and 40 μl sodium ascorbate (0.1 M) was added, purged again with N_2 for 0.5 min, before stirring at room temperature for 1 h under a N_2 atmosphere. The resulting dextran conjugate was diluted with milliQ water and washed with the 10% acetonitrile to remove excess compound 8 using an Amicon filter (MWCO, 3 kDa).

Self-assembly of I^{A647}_{FD}. Half icosahedrons (VU₅ and VL₅) was prepared as described in the literature^{56,57}. To synthesize the DNA-icosahedron, VU₅ and VL₅ (3 μM each, 30 μl , in 50 mM phosphate buffer, pH 6.0) containing 2 mM solution of the compound 8 conjugated dextran (FD) ($M_w \sim 10$ kDa) was mixed in an Eppendorf tube and heated to 37 °C for 30 min. The temperature was reduced to 20 °C at a rate of 1 °C per 3 min and followed by incubation for 2 h. The reaction mixture was transferred to a refrigerator at 4 °C for further incubation for longer time periods up to 48 h. The formation of I^{A647}_{FD} was characterized by 0.8 wt% agarose gel electrophoresis (Supplementary Fig. 3a).

Preparation of I^{A647}_{FD-ON}. A solution (10 μl , 3 μM) of I^{A647}_{FD} was treated with 1 μl (5 mM) NaSH solution in 0.1 M phosphate buffer at pH 7.4 and stirred for 2 h at room temperature. The excess thiol was removed by ultracentrifugation using an Amicon filter (MWCO, 3 kDa).

Determination of the size of different thiols. Dynamic light scattering (DLS) experiments were carried out using a Wyatt Dynapro Nanostar Plate Reader. Samples were dissolved in milliQ water or buffer filtered through 0.22 μm filter to remove dust particles. Samples were illuminated with a laser wavelength of 658 nm, at a sensitivity of 80%, and with a scattering angle set at 90° with a 10 s acquisition time for data collection. The percentage intensity observed for each sample was plotted against the respective hydrodynamic radius (R_h) values. The sizes of PEG-SH (3.2 kDa), Dex-SH (10 kDa) and Dex-SH (40 kDa) were determined from

DLS measurements. An aqueous solution of the free thiol-containing polymer (1 mg ml⁻¹) was filtered in a dust-free environment, and DLS measurements were carried out with this solution. For GSH, cysteine and H₂S we used Chem 3D Ultra 8.0 software and used the end to end distance of the energy minimized structure as the diameter of those molecules.

In vitro fluorescence measurements. Fluorescence spectra were recorded on a FluoroMax-4 instrument (Horiba Jobin Yvon). TDX and TDX_{OFF} reporter were diluted to 100 nM in 0.1 M phosphate buffer at pH 7.2 in the presence or absence of 5 mM GSH. The samples were excited at 450 nm (for fluorescein emission) and 575 nm (for Rhodamine emission). The emission spectra were collected in the ranges 460–600 nm and 590–700 nm for fluorescein and Rhodamine, respectively, at different time points. Three independent measurements were recorded for each sample (Fig. 1c).

We checked the specificity of the reporter dye towards the thiol–disulfide exchange reaction. We treated the reporter dye (compound 8) with different metal ions and amino acids. No reaction was observed with any of the metal ions and amino acids tested except cysteine (Supplementary Fig. 1c).

To check the substrate availability for the disulfide exchange reaction with I^{A647}_{FD} as a function of the size of the reactive thiols (1 mM), we treated I^{A647}_{FD} (3 μM) and FD with various thiols and checked the emission spectra after 1 h of incubation. To monitor the spectra, the samples were excited at 450 nm (fluorescein channel) and 647 nm (Atto 647N channel). The emission spectra were collected in the ranges 460–600 nm and 650–750 nm for fluorescein and Atto 647N, respectively (Supplementary Fig. 3b).

Protocols for C. elegans and strains. Standard methods for the maintenance of *C. elegans* were followed. We used a wild-type *C. elegans* strain isolated from Bristol (strain N2). All strains were obtained from the Caenorhabditis Genetics Center (CGC). The mutant strain used for the experiment was VC586 [*pdi-1(gk271) III*].

The transgenic strains used for this study are as follows:

- cdIs131 [pcc1::GFP::rab-5 + unc-119(+)+ myo-2p::GFP]*, a transgenic strain that express GFP-fused early endosomal marker RAB-5 inside coelomocytes;
- cdIs66 [pcc1::GFP::rab-7 + unc-119(+)+ myo-2p::GFP]*, a transgenic strain that express GFP-fused late endosomal/lysosomal marker RAB-7 inside coelomocytes;
- pwl50 [lmp-1::GFP + Cbr-unc-119(+)]*, a transgenic strain that express GFP-fused lysosomal marker LMP-1;
- dvIs70 [hsp-16.2p::GFP + rol-6(su1006)]*, a transgenic strain that shows GFP expression under heat shock protein HSP-16.2 promoter (it expresses GFP in the presence of mild heat shock).

Protocols for C. diphtheria strains and growth conditions. Two different types of *C. diphtheria* strain were used for pathogen infection to *C. elegans*: the toxic *C. diphtheria* (ATCC 13812), which produces diphtheria toxin and the less toxic *C. diphtheria* (ATCC 39526) (DT Δ 149), which produces mutated diphtheria toxin. For toxic and less toxic *C. diphtheria* we used tryptic soy broth with 5% sheep blood and ATCC medium and 1417 low iron yeast extract with casamino acid as culture medium, respectively, and inoculated for 24 h at 37 °C as described on the ATCC website.

TDX and I^{A647}_{FD} reporters targeted to coelomocyte of C. elegans. For coelomocyte targeting⁵⁶ we microinjected 2 μM of TDX reporter in the dorsal side in the pseudocoelom, just opposite the vulva, of 1-day-old wild-type hermaphrodites. Injected worms were then placed in a new nematode growth medium (NGM) agar-containing Petri plate at 22 °C for incubation at different time points. They were then mounted on an agar pad (2.0%) and anaesthetized using 40 mM sodium azide in M9 buffer, before being subjected to the fluorescence imaging experiment. The same protocol was followed for TDX_{OFF} and TDX_{ON}.

DNA-icosahedron encapsulated reporters, (I^{A647}_{FD}, I^{A647}_{FD-ON} and I^{A647}_{FD-OFF}, 3 μM each) were injected into wild-type worms as described earlier and imaged at 30 min post-injection.

Co-localization of TDX^R with late endosomes in coelomocytes. To investigate the localization of the TDX reporter at 20 min post injection, we conducted a co-localization experiment using *cdIs131*, *cdIs66* and *pwl50* transgenic worms. We injected 2 μM Rhodamine DNA duplex into the worms and imaged after 20 min. Approximately 85% co-localization of TDX reporter with RAB-7::GFP positive vesicles was observed, which marks late endosomal and lysosomal compartments (Fig. 2d and Supplementary Fig. 8).

RNAi experiment. We used BLASTP⁶³ to look for thioredoxin domain-containing protein in the *C. elegans* genome. Bacteria of interest, expressing double-stranded RNA (Supplementary Table 2), were obtained from Ahringer RNAi library⁵⁸ and Vidal Unique⁵⁹. Cloned bacteria were fed to the worms and ~60 one-day adults of the F1 progeny were used for screening. The Ahringer or Vidal unique library did not contain bacterial clones for *Y73B6BL.2* and hence this gene was not included in the screen.

The mRNA levels of the candidate genes were assayed by RT-PCR²⁸. Briefly, we isolated total RNA using the trizol-chloroform method; 2.5 µg of total RNA was converted to cDNA using oligo-dT primers, and a 5 µl volume of the reverse transcription reaction was used to set up PCR using gene-specific primers. The PCR products were analysed on a 1.5% agarose-tris-acetate-EDTA gel (Fig. 3c). The sizes of the PCR products expected for each gene were as follows: actin (360 bp), *pdi-3* (682 bp), *C30H7.2* (798 bp), *trx-2* (316 bp) and *trx-1* (261 bp).

***hsp-16.2::GFP* experiments to measure diphtheria toxin infection-triggered translational inhibition.** *hsp2::GFP* experiments were modified from a literature-reported procedure⁴². Briefly, fresh cultures of either toxic or less toxic *C. diphtheria* (DTΔ149) were seeded into an NGM-containing agar plate. Each plate contained 50 µl of bacterial culture. The plates were kept at 25 °C for 24 h to dry the liquid medium on agar. Wild-type or different genetic background worms were washed onto *C. diphtheria* seeded plates and incubated for 6 h for infection at 25 °C, then washed and transferred to a plate containing OP50 or the bacteria carrying the RNAi clone. These *C. elegans* were then subjected to 1 h heat shock at 37 °C and then returned to 25 °C for another 1 h. The worms were imaged for GFP expression, which was quantified by keeping the microscope settings fixed for all samples. A standard region of the pharynx and intestine was chosen for GFP intensity measurements (Supplementary Fig. 6). For the intestine we chose a region towards the posterior of the intestine because it showed robust GFP expression. GFP intensity was measured for at least 20 worms in each genetic background.

Cell culture. HeLa cells were a gift from C. He (Department of Chemistry, University of Chicago). Mouse macrophages J774A.1 cells were a gift from D. J. Nelson (Department of Pharmacological and Physiological Sciences, University of Chicago). The cells were cultured in DMEM-F12 with 10% FBS, 100 U ml⁻¹ penicillin and 100 µg ml⁻¹ streptomycin and maintained at 37 °C under 5% CO₂.

Bone marrow derived macrophages (BMDMs) were isolated from the femurs and tibias of male C57BL/6 mice, obtained from the laboratory of L. Becker (Ben May Department for Cancer Research, University of Chicago). Cells were differentiated to macrophages using murine macrophage colony-stimulating factor (M-CSF) for 6 days. For lipopolysaccharides (LPS) activation, cells were treated with 20 ng ml⁻¹ LPS for 24 h. All animal studies were in compliance with ethical regulations approved by the University of Chicago Institutional Animal Care and Use Committee (ACUP 72209).

Microscopy and ratiometric image analysis. Wide-field microscopy was performed on an IX83 inverted microscope (Olympus) using a ×60, 1.42 NA, phase contrast oil immersion objective (PLAPON, Olympus) and Evolve Delta 512 electron-multiplying charge-coupled device (EMCCD) camera (Photometrics). The filter wheel, shutter and CCD camera were controlled using Metamorph Premier Version 7.8.12.0 (Molecular Devices), as appropriate for the fluorophore used. Images were acquired on the same day under the same acquisition settings. Confocal imaging was carried out on a Leica SP5 II STED-CW super-resolution microscope, using an argon ion laser for 488 nm excitation and diode-pumped solid-state laser (DPSS) for 561 nm excitation with a set of dichroic, excitation and emission filters suitable for each fluorophore. Crosstalk and bleed-through were measured and found to be negligible between GFP/fluorescein and Rhodamine.

All images were background subtracted using the mean intensity calculated from an adjacent cell-free area. Fluorescein and Rhodamine images were co-localized, and endosomes showing good co-localization were analysed using ImageJ-Win64 software (NIH). Mean fluorescence intensity in each endosome was measured in fluorescein (G) and Rhodamine (R) channels. The ratio of the G/R intensities was calculated from these values. Pseudocolour images were generated by measuring the G/R ratio per pixel. Using ImageJ software, pixels were then colour coded to indicate differences between high and low G/R ratios.

Percentage response calculation. The percentage responses of the TDX reporter at different time points for the wild-type worm and the RNAi worm (20 min) were calculated using equation (1):

$$\% \text{ Response} = \left[\frac{(G/R)_{\text{TDX}_{\text{OFF}}} - (G/R)_{\text{TDX}_{\text{ON}}}}{(G/R)_{\text{TDX}_{\text{ON}}} - (G/R)_{\text{TDX}_{\text{OFF}}}} \right] \times 100 \quad (1)$$

where $(G/R)_{\text{TDX}}$, $(G/R)_{\text{TDX}_{\text{OFF}}}$ and $(G/R)_{\text{TDX}_{\text{ON}}}$ indicate the observed fluorescence intensity ratio of fluorescein to Rhodamine at a given time point by using TDX, TDX_{ON} and TDX_{OFF} reporters, respectively.

Targeting TDX reporter to endolysosomal pathway in HeLa cells. We incubated HeLa cells with TDX reporter (1 µM) containing DMEM without FBS for 1 h at 37 °C. Cells were then washed with PBS (pH 7.4) three times to remove any uninternalized TDX nanodevice and then incubated for various chase times in DMEM complete medium. Before imaging, cells were washed with PBS and imaged in Hank's balanced salt solution (GE Healthcare) buffer. A similar protocol was followed for TDX_{ON} and TDX_{OFF} reporters.

RNAi knockdown and pharmacological inhibition in HeLa cells. All relevant siRNAs were obtained from Dharmacon. HeLa cells were split on an imaging dish at 1 × 10⁴ seeding density. After 16 h in culture, the cells were transfected with siRNAs using DharmaFECT1 (Dharmacon; cat. no. T-2001-01) transfection reagent according to the manufacturer's protocol. For Erp57 and TRX-1 knockdown, HeLa cells were transfected with Erp57 siRNA⁶⁰ (5'-GGGCAAGGACUUAUUUUTT-3') and TRX-1 siRNA (Dharmacon; cat. no. M-006340-010005). As a negative control, we used negative control siRNA (Dharmacon; cat. no. D-001210-01-05). After 72 h of transfection, cells were incubated with the tripartite TDX reporter for 1 h in DMEM without FBS and chased for 3 h in complete medium and imaged as described earlier.

For pharmacological inhibition, cells were incubated with complete medium containing either NEM (10 µM) or DTNB (100 µM) for 1 h, followed by 1 h of incubation with TDX reporter in DMEM without FBS. The cells were chased for 4 h in complete medium containing either 10 µM NEM or 100 µM DTNB, washed with PBS and imaged as described in HBSS buffer containing either 10 µM NEM or 100 µM DTNB so that the relevant pharmacological inhibitor was always present.

Cathepsin C activity assay. J774A.1 cells with or without cathepsin inhibitor E64 were pulsed with 500 nM of either *Cat* or *Cat*_{ON} probes (Supplementary Figs. 14 and 15) separately for 30 min at 37 °C. After 1 h, cells were washed and imaged in the Rhodamine (G, λ_{em} = 520 nm) and Alexa 647 (R, λ_{em} = 670 nm) channels. The *Cat*_{ON} probe provided the maximum possible ratiometric signal (G/R) if the *Cat* probe was completely cleaved. All G/R values were normalized to that of *Cat*_{ON}. Similar pulse and chase experiments were performed in BMDMs with 200 nM *Cat* probes. BMDMs were then subjected to flow cytometry on a FACSCanto II flow cytometer (Supplementary Fig. 15).

Statistical analysis. We used the Graphpad unpaired *t*-test calculator for all statistical significance calculations (<https://www.graphpad.com/quickcalcs/ttest1/>).

Reporting summary. Further information on research design is available in the Nature Research Reporting Summary linked to this article.

Data availability

The data that support the plots within this paper and other finding of this study are available from the corresponding author upon reasonable request.

References

- Presolski, S. I., Hong, V. P. & Finn, M. G. Copper-catalyzed azide-alkyne click chemistry for bioconjugation. *Curr. Protoc. Chem. Biol.* **3**, 153–162 (2011).
- Bhatia, D., Surana, S., Chakraborty, S., Koushika, S. P. & Krishnan, Y. A synthetic icosahedral DNA-based host-cargo complex for functional *in vivo* imaging. *Nat. Commun.* **2**, 339 (2011).
- Veetil, A. T. et al. Cell-targetable DNA nanocapsules for spatiotemporal release of caged bioactive small molecules. *Nat. Nanotechnol.* **12**, 1183–1189 (2017).
- Kamath, R. S. & Ahringer, J. Genome-wide RNAi screening in *Caenorhabditis elegans*. *Methods* **30**, 313–321 (2003).
- Rual, J.-F. et al. Toward improving *Caenorhabditis elegans* phenome mapping with an ORFeome-based RNAi library. *Genome Res.* **14**, 2162–2168 (2004).
- Xu, D., Perez, R. E., Rezaiekhaliq, M. H., Bourdi, M. & Truong, W. E. Knockdown of ERp57 increases BiP/GRP78 induction and protects against hyperoxia and tunicamycin-induced apoptosis. *Am. J. Physiol. Lung Cell. Mol. Physiol.* **297**, L44–L51 (2009).

Reporting Summary

Nature Research wishes to improve the reproducibility of the work that we publish. This form provides structure for consistency and transparency in reporting. For further information on Nature Research policies, see [Authors & Referees](#) and the [Editorial Policy Checklist](#).

Statistical parameters

When statistical analyses are reported, confirm that the following items are present in the relevant location (e.g. figure legend, table legend, main text, or Methods section).

n/a Confirmed

- The exact sample size (n) for each experimental group/condition, given as a discrete number and unit of measurement
- An indication of whether measurements were taken from distinct samples or whether the same sample was measured repeatedly
- The statistical test(s) used AND whether they are one- or two-sided
Only common tests should be described solely by name; describe more complex techniques in the Methods section.
- A description of all covariates tested
- A description of any assumptions or corrections, such as tests of normality and adjustment for multiple comparisons
- A full description of the statistics including central tendency (e.g. means) or other basic estimates (e.g. regression coefficient) AND variation (e.g. standard deviation) or associated estimates of uncertainty (e.g. confidence intervals)
- For null hypothesis testing, the test statistic (e.g. F , t , r) with confidence intervals, effect sizes, degrees of freedom and P value noted
Give P values as exact values whenever suitable.
- For Bayesian analysis, information on the choice of priors and Markov chain Monte Carlo settings
- For hierarchical and complex designs, identification of the appropriate level for tests and full reporting of outcomes
- Estimates of effect sizes (e.g. Cohen's d , Pearson's r), indicating how they were calculated
- Clearly defined error bars
State explicitly what error bars represent (e.g. SD, SE, CI)

Our web collection on [statistics for biologists](#) may be useful.

Software and code

Policy information about [availability of computer code](#)

Data collection

FluorEssence Horiba for fluorescence measurements, MetaMorph for Olympus and LAS_AF Leica confocal software for image acquisition, Image Lab™ Software 6.0.0 for PAGE image acquisition

Data analysis

Origin (OriginLab, Northampton, MA) for image analysis, ImageJ/Fiji 1.52e for image analysis

For manuscripts utilizing custom algorithms or software that are central to the research but not yet described in published literature, software must be made available to editors/reviewers upon request. We strongly encourage code deposition in a community repository (e.g. GitHub). See the Nature Research [guidelines for submitting code & software](#) for further information.

Data

Policy information about [availability of data](#)

All manuscripts must include a [data availability statement](#). This statement should provide the following information, where applicable:

- Accession codes, unique identifiers, or web links for publicly available datasets
- A list of figures that have associated raw data
- A description of any restrictions on data availability

The data that support the plots within this paper and other finding of this study are available from the corresponding author upon reasonable request.

Field-specific reporting

Please select the best fit for your research. If you are not sure, read the appropriate sections before making your selection.

Life sciences Behavioural & social sciences Ecological, evolutionary & environmental sciences

For a reference copy of the document with all sections, see [nature.com/authors/policies/ReportingSummary-flat.pdf](https://www.nature.com/authors/policies/ReportingSummary-flat.pdf)

Life sciences study design

All studies must disclose on these points even when the disclosure is negative.

Sample size	Sample size was determined based on adequate representation of the population. Replicates were performed to ensure reproducibility.
Data exclusions	No data were excluded from the analyses
Replication	In vitro fluorescence assay, experiments related to percentage response calculation of the reporter inside live <i>C. elegans</i> as well as in cells are done in triplicate. <i>C. elegans</i> infection assay was replicated in duplicates. The data was reproducible in all cases and representative data was shown.
Randomization	NGM plates containing worms as well as cultured dishes containing various types of cells were randomized for selection in imaging experiments and biochemical assays.
Blinding	No formal blinding was done for these assays.

Reporting for specific materials, systems and methods

Materials & experimental systems

n/a	Involvement in the study
<input checked="" type="checkbox"/>	<input type="checkbox"/> Unique biological materials
<input checked="" type="checkbox"/>	<input type="checkbox"/> Antibodies
<input type="checkbox"/>	<input checked="" type="checkbox"/> Eukaryotic cell lines
<input checked="" type="checkbox"/>	<input type="checkbox"/> Palaeontology
<input type="checkbox"/>	<input checked="" type="checkbox"/> Animals and other organisms
<input checked="" type="checkbox"/>	<input type="checkbox"/> Human research participants

Methods

n/a	Involvement in the study
<input checked="" type="checkbox"/>	<input type="checkbox"/> ChIP-seq
<input type="checkbox"/>	<input checked="" type="checkbox"/> Flow cytometry
<input checked="" type="checkbox"/>	<input type="checkbox"/> MRI-based neuroimaging

Eukaryotic cell lines

Policy information about [cell lines](#)

Cell line source(s)	HeLa cells were a kind gift from Prof. Chuan He, Department of Chemistry, the University of Chicago. Mouse alveolar macrophage J774A.1 cells were a kind gift from Prof Deborah Nelson, Department of Pharmacological and Physiological Sciences, the University of Chicago.
Authentication	HeLa cells and J774.1 cells were authenticated by short tandem repeats (STR) prior to receiving the cells as a gift.
Mycoplasma contamination	We routinely check our cell lines for Mycoplasma contamination using Hoechst staining and all three cell lines used in this study turned out to be negative for Mycoplasma contamination.
Commonly misidentified lines (See ICLAC register)	No commonly misidentified cell lines were used.

Animals and other organisms

Policy information about [studies involving animals](#); [ARRIVE guidelines](#) recommended for reporting animal research

Laboratory animals	<i>C. Elegans</i> strains and male C57BL/6 mice were used in this study. Details of all worm strains used are provided in the Online methods under the section "Protocols for <i>C. elegans</i> and strains"
Wild animals	Study did not involve any wild animals.

Field-collected samples

Study did not involve samples collected from field.

Flow Cytometry

Plots

Confirm that:

- The axis labels state the marker and fluorochrome used (e.g. CD4-FITC).
- The axis scales are clearly visible. Include numbers along axes only for bottom left plot of group (a 'group' is an analysis of identical markers).
- All plots are contour plots with outliers or pseudocolor plots.
- A numerical value for number of cells or percentage (with statistics) is provided.

Methodology

Sample preparation

Bone marrow cells were isolated from C57BL/6 mice and differentiated into BMDM. On day 6, use IFN γ and LPS to stimulate them into M1- or IL4 into M2-BMDM for 24hrs. Cells were then incubated with 200nM Cath probe for 30 mins followed by washing the cells and another 30min incubation. These cells were then used for flow cytometry.

Instrument

Samples were analyzed using a FACSCanto™ II flow cytometer.

Software

Data were quantified by FlowJo v.10.4.1.

Cell population abundance

All cells are BMDM.

Gating strategy

Cells were gated by FSC/SSC for total population; SSC-A/SSC-H for single cells; cblue labeling for live cells population followed by geometric mean (MFI) calculation for APC (uptake) and FITC (uptake) histogram.

- Tick this box to confirm that a figure exemplifying the gating strategy is provided in the Supplementary Information.